

Supplementary Information

Cellulase mimicking nanomaterial-assisted cellulose hydrolysis for enhanced bioethanol fermentation: an emerging sustainable approach

Mamata S. Singhvi, Aarti R. Deshmukh, Beom Soo Kim*

**Department of Chemical Engineering, Chungbuk National University, Chungbuk,
Republic of Korea**

TABLE OF CONTENTS	
MATERIALS AND METHODS	02
RESULTS AND DISCUSSION.....	06
SUPPORTING FIGURES.....	07
SUPPORTING TABLES.....	14
REFERENCES	17

Materials and Methods

S1. Nanomaterial synthesis: All the listed twelve nanomaterials used during screening were prepared by using plant extracts as described here.

Preparation of plant extract: Aqueous plant extract was prepared by the following procedure: 1.0 g of powdered plant material was mixed with 100 ml of distilled water and heated at 95 °C while stirring continuously at 300 rpm for 1 h. The resulting plant extract solution was filtered using the Whatman filter paper and then centrifuged at 10,000 rpm for 20 min. The extract was stored in the refrigerator for further use to synthesize nanoparticles and exfoliation of boron nitride and expanded graphite.

1. Preparation of iron oxide nanoparticles (FeNPs)

FeNPs were synthesized by the co-precipitation method with slight modification as reported previously.¹ Initially, 10 ml of fenugreek seed extract (prepared according to the plant extract preparation method mentioned above) was added to 50 ml of 1 M FeCl₂ and 2 M FeCl₃, followed by stirring at room temperature for 3 h. Later, 1 ml of 25% ammonia solution was added to the suspension under continuous stirring for 1 h. The nanoparticles were separated by magnet to remove unreacted reactant and the separated nanoparticles were washed several times with distilled water and dried in hot air oven at 60 °C.

2. Preparation of iron oxide sodium alginate beads (FeSAlg)

FeSAlg were prepared by sol-gel method using sodium alginate and calcium chloride system. 1.0 g of FeNPs was mixed in 100 ml of 1% sodium alginate solution for 24 h. Then, this FeNPs and sodium alginate solution were dropwise added into 4% CaCl₂ bath. When sodium alginate comes into contact with CaCl₂, gelation occurs at the interface of the drop and the spherical structure is formed. Furthermore, these beads were allowed to stir in CaCl₂ bath till 4 h for complete gelation. After 4 h, beads were separated using magnet, washed several times with distilled water, and freeze dried for further use.

3. Preparation of silver nanoparticles (AgNPs)

AgNPs were prepared using fenugreek seed extract as a reducing and capping agent as reported previously.¹ In a typical experiment, 5.0 ml of fenugreek seed extract was added dropwise into 50 ml of 1 mM silver nitrate solution in a round bottom flask covered with aluminium foil under continuous stirring at room temperature for 4 h. As the reaction proceeded, the colour of solution was changed from colourless to pale yellow to brown, which suggested the formation of AgNPs. Finally, obtained AgNPs were centrifuged at

10,000 rpm for 30 min followed by washing with distilled water and finally lyophilization for dried AgNPs.

4. Preparation of silver nanoparticles sodium alginate beads (AgSAlg)

In a typical experiment, 2% of sodium alginate was mixed with 100 ml of gallnut extract. Then, alginate was allowed to homogenize in gallnut extract at room temperature for 24 h. Then this solution was dropped into 1 mM AgNO₃ bath at a rate of 1 ml/min. Then, the mixture was slowly stirred under magnetic stirring for 1 h. The beads coated with AgNPs were separated from the solution, washed with distilled water, and freeze dried for further use.

5. Preparation of gold nanoparticles (AuNPs)

1.0 ml of a freshly prepared gallnut extract was added dropwise in a flask containing 100 ml of 1 mM HAuCl₄ solution. Upon addition of gallnut extract, light yellow coloured HAuCl₄ solution turned to red wine colour in 2 min. This change in colour of solution confirmed the formation of AuNPs. Stirring was further continued for 30 min, then the resulting solution was centrifuged at 10,000 rpm and settled AuNPs were washed with distilled water. To get dried AuNPs, the nanoparticle solution after washing was freeze dried and used for further experiments.

6. Preparation of gold nanoparticles sodium alginate beads (AuSAlg)

In a typical experiment, 2% of sodium alginate was mixed with 100 ml of gallnut extract. This gallnut extract mixed alginate solution were allowed to homogenize at room temperature for 24 h. Then, the completely homogenized solution was dropped at a rate of 1 ml/min into the beaker containing 500 ml of 1 mM HAuCl₄ and 4% CaCl₂ (1:1) solution. Then, the mixture of beads in bath was stirred continuously under magnetic stirring for 2 h. Finally, the beads were separated from the solution, washed with distilled water, and freeze dried for further use.

7. Preparation of boron nitride nanosheets (BNNs)

Boron nitride (BN) was subjected to an ultrasonic liquid exfoliation method as reported in our previous study.² Briefly, 2.5 g of BN powder was added to 500 ml of gallnut extract and the mixture was sonicated for 24 h at 30 °C. After sonication, the solution was allowed to stand overnight for settling unexfoliated BN. The resulting suspension was centrifuged at 10,000 rpm to obtain the exfoliated BNNs, followed by freeze drying to obtain BNNs.

8. Preparation of carbon nitride nanosheets (CNNs)

CNNs were prepared using melamine as reported by Cheng et al.³ Melamine was heated at 550 °C for 2 h under air condition with a ramp rate of about 5 °C/min for the heating process

to obtained yellow products, bulk g-C₃N₄. g-C₃N₄ nanosheets (CNNs) were prepared by exfoliation of as prepared bulk g-C₃N₄ in water. Briefly, 0.1 g of bulk g-C₃N₄ powder was dispersed in 100 ml of water and the mixture was sonicated for 24 h. The resulting suspension was centrifuged at 6000 rpm to remove the residual non-exfoliated g-C₃N₄, followed by centrifugation at 15,000 rpm to obtain CNNs. Then, these CNNs were freeze dried and used for further experimentation.

9. Preparation of functionalized few-layer graphene (FFG)

FFG was prepared using liquid phase exfoliation of expanded graphite as reported previously.^{4,5} Here, 1.0 g of expanded graphite was exfoliated using gallnut extract as an exfoliating solvent in bath sonicator for 24 h at 30 °C by maintaining cooling water circulation. The resulting solution was allowed to sediment for 12 h to enable separation of large non-exfoliated flakes, followed by centrifugation of supernatant at 15,000 rpm to obtain FFG. In order to remove unbound gallnut extract from FFG sheets, these FFG was further washed with distilled water, and lastly centrifuged at 10,000 rpm for 30 min and freeze dried to get powdered FFG.

10. Preparation of gold nanoparticle-functionalized few-layer graphene (AuFFG)

AuFFG nanohybrid was synthesized using FFG fabricated as in method 9. 100 mg of FFG was dispersed in 50 ml distilled water under a continuous stirring at room temperature for 30 min. The resulting solution was sonicated for 10 min in bath sonicator at mild sonication. Again, the sample was kept for continuous stirring at 200 rpm. Then, 50 ml of 1 mM HAuCl₄.3H₂O was added dropwise. For complete reduction of Au³⁺ ions onto FFG, this mixture was continuously stirred for 4 h. It was observed that with mixing time, colour of solution changed from light brown to brownish purple, suggesting the formation of Au on FFG. Further, the obtained dispersion was centrifuged at 10,000 rpm and settled pellet was washed to remove unreacted HAuCl₄. The resulting AuFFG nanohybrids were freeze dried and used for further characterization and experimentation.

11. Preparation of silver nanoparticles-functionalized few-layer graphene (AgFFG)

AgFFG nanohybrid was prepared by following the similar method as mentioned above for AuFFG using 1 mM AgNO₃ solution instead of HAuCl₄.3H₂O.

S2. Fabrication of raw and treated CC/chitosan composite films

1. DPPH radical scavenging activity (%)

DPPH assay is a simple, acceptable, and most widely used technique to evaluate radical scavenging potency of antioxidant properties of test sample.⁶ DPPH radical scavenging activity was determined following a protocol described by previously reported work with slight modification.⁷ The scavenging activity of all treated CC samples and CC/chitosan composite films were determined by measuring absorbance of methanolic DPPH solution at 517 nm. DPPH solution (0.1 mM) was prepared in methanol. Then, 1 ml DPPH solution and 0.5 ml sample solution (0.001 mg/ml of powder treated CC and 5×5 mm film) were mixed, and incubated at 37 °C for 30 min. After 30 min, eppendorf tubes containing the reaction mixture were centrifuged and absorbance of supernatant was measured using BIO-RAD spectrophotometer. Absorbance was compared with blank DPPH and scavenging activity was calculated using equation (1).

$$DPPH\ scavenging\ activity\ (\%) = \left(1 - \frac{A_{Sample\ at\ 517nm}}{A_{Control\ at\ 517nm}}\right) \times 100 \quad (1)$$

2. Light transmittance and opacity of films

Light transmittance and opacity of the chitosan and CC/chitosan composite films were measured using a UVmini-1240 spectrophotometer in the wavelength range of 200-800 nm. Empty cuvette was used as reference. Films transmittance was determined by placing the film sample in cuvette, perpendicular to the direction of light source. Films opacity was determined by measuring absorbance at 600 nm and determined using equation (2):

$$Opacity = \frac{A_{600}}{x} \quad (2)$$

where A_{600} is the absorbance at 600 nm wavelength and x is the thickness of the film (mm).⁸

3. Mechanical properties of film sample

Mechanical properties of all films were determined in terms of tensile strength (MPa) and elongation at break (%) according to ASTM D882 standard method using universal materials testing machine (UTM, TW QC-506M1 20kN). Film samples were cut into 10 mm × 50 mm rectangular strips. Films were held parallel with an initial separation set at 20 mm using cell load of 5 kN with cross head speed of 5 mm/min. Three replications of each film type were tested.⁶

S3. Preparation of FFG/polyvinyl alcohol (PVA) aerogel

A 10% PVA aqueous solution was prepared in round bottom flask by refluxing at 95 °C for 3 h. Separately, FFG in 5 ml water was sonicated for 15 min, then mixed with 5 ml of 10% PVA and stirred for 2 h for proper mixing. To get rid of air bubbles, the resulting homogeneous solution was sonicated in a water bath for 20 min at 30 °C. Then, 2 ml of FFG/PVA solution was poured into a 24-well plate and subjected to five cyclic freeze/thaw processes consisting of a freezing step at -20 °C for 20 h and thawing step for 4 h at room temperature.⁹ The obtained hydrogel was freeze dried to get an aerogel. PVA aerogel was prepared following the same procedure of FFG/PVA without addition of FFG.

S4. Results and Discussion

(A) Scanning electron microscopy (SEM) and energy dispersive X-ray spectrophotometry (EDX) analysis

The scanning electron microscopy images as shown in **Fig. S1A** describe the shape and the surface morphology of twelve materials used in the present work. SEM image of FeNPs showed nanostructure of spherical shape. Highly porous and wrinkle surface can be observed on the surface of FeSAIlg beads. AgNPs showed cube shape. AgSAIlg displayed the high surface area of beads. AuNPs showed the spherical shape of uniform size. AuSAIlg displayed the similar surface morphology as that of FeSAIlg beads. Disc-like flat nanosheets of BNNs and CNNs can be clearly observed in SEM micrograph. SEM image of expanded graphite showed the thick flake of an average size of ~95 µm. Further, exfoliation led to FFG in thin sheet form as shown in the microscopic image. The distortion of expanded graphite observed in SEM is mostly due to ultrasonicated exfoliation and functionalization with oxygen-containing functional groups. AuFFG and AgFFG showed the formation of nanoparticles on the FFG sheets.

Further, the elemental composition of the twelve nanomaterials characterized using EDX confirmed the presence of specific metallic component, carbon, oxygen, and other elements in each nanomaterial along with their purity. As shown in **Fig. S1B**, strong signals for specific metal Fe: 0.65 eV; Ag: 0.3, 2.97 eV; Au: 0.24, 2.07 eV; B: 0.11 eV; N: 0.39 eV; C: 0.27 eV, and O: 0.52 eV, confirm the formation of desired nanomaterials.⁵ In nanoparticle samples, some carbon and oxygen peaks may originate from the biomolecules that are bound to the surface of nanoparticles. Additionally, Ca: 0.24 eV, Na: 1.01 eV, and Cl: 0.24, 3.65 eV were also observed in FeSAIlg, AuSAIlg, and AgSAIlg, due to the sol-gel interaction of sodium alginate with calcium chloride. The details of elemental composition of all nanomaterials are

given in **Table S1**.

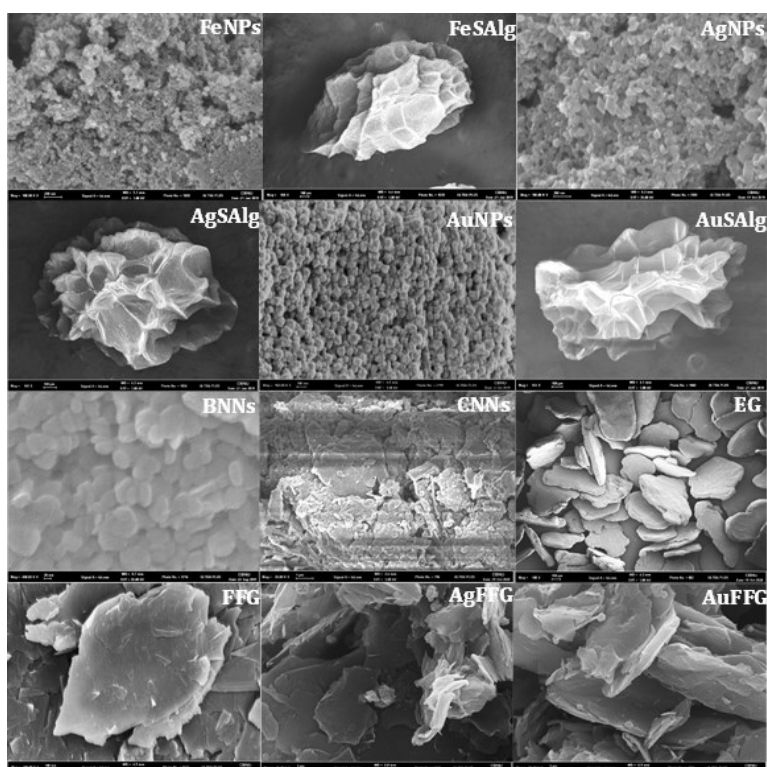


Fig. S1A SEM images of twelve nanomaterials used for screening studies

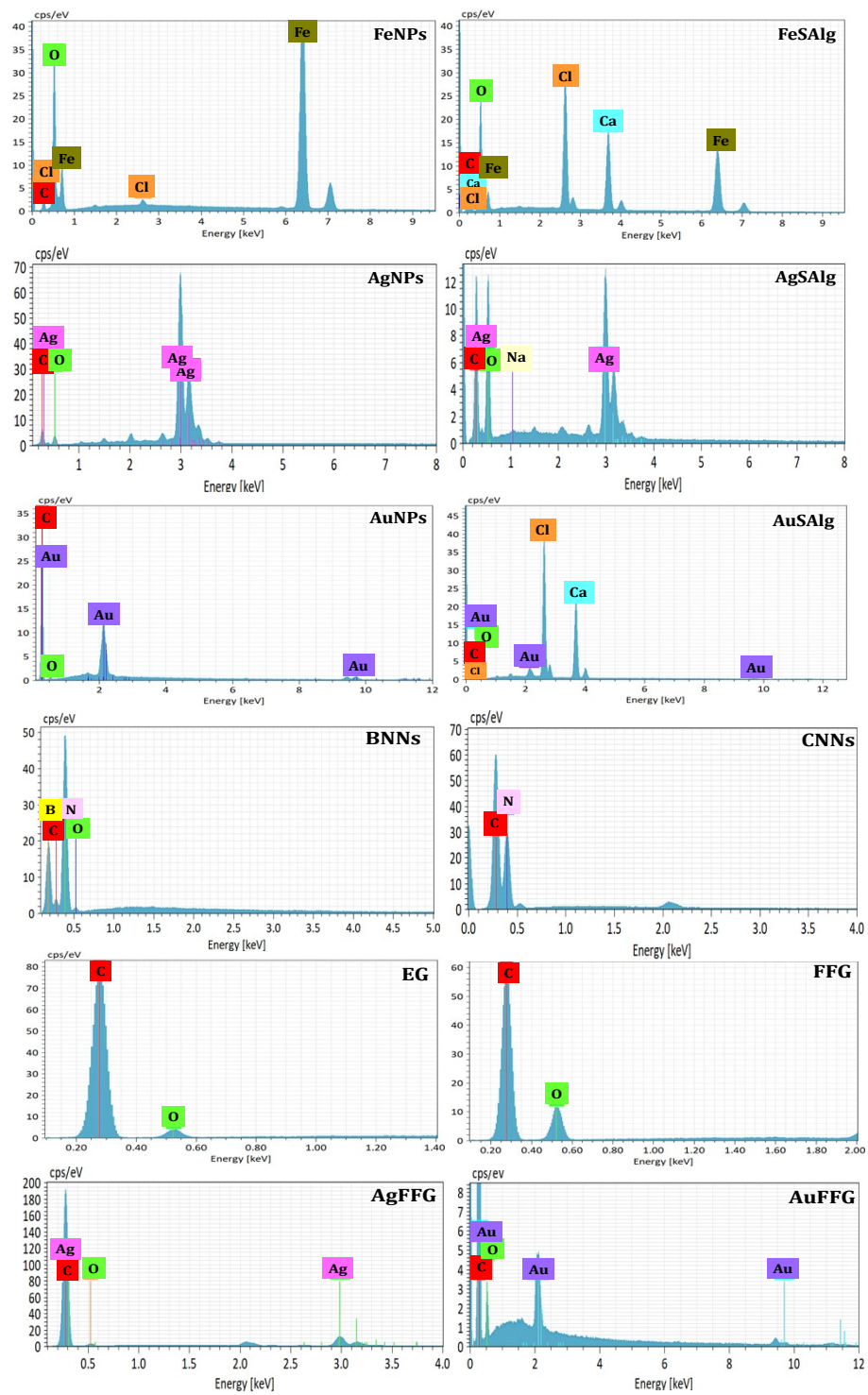


Fig. S1B EDX analysis of twelve nanomaterials used for screening studies

(B) Fourier transform-infrared (FTIR) spectroscopy and X-ray analysis

FTIR analysis of nanomaterials confirms the formation of nanomaterials and provides the detail information about the functional groups associated with them. In this study, all nanomaterials were synthesized using plant extract. In **Fig. S2A**, FTIR of all nanomaterials synthesized using plant extract showed fingerprints of various functional groups. The strong –OH peak is observed at $\sim 3421\text{ cm}^{-1}$. Asymmetric C-H stretching and carboxylic group vibration is observed at 2311 cm^{-1} and 1716 cm^{-1} . The stretching of C=C and secondary amine protein's bending vibration are observed at 1613 cm^{-1} and 1547 cm^{-1} , respectively. Aromatic groups, C-C stretching vibrations are observed at 1453 cm^{-1} . Stretching of hydroxyl and carboxylate groups are observed at 1331 cm^{-1} . The stretching mode polyol C-O is observed at 1204 cm^{-1} .

The crystallographic nature of the all green synthesized nanomaterials was determined by XRD analysis and shown in **Fig. S2B**. The typical XRD patterns of FeNPs and FeSAlg (**Fig. S2B**) showed distinct peaks of iron oxide nanoparticles, indexed at 29.7 , 34.3 , 41.7 , 53.1 , 56.8 , and 61.8° representing (220), (311), (400), (422), (511), and (440) crystallographic planes. From the XRD spectra of AgNPs and AgSAlg (**Fig. S2C**), distinct peaks at 37.8 , 44.1 , 65.1 , 76.2 , and 80.7° are indexed as (111), (200), (220), and (311) planes of face centered cubic AgNPs. XRD pattern of AuNPs and AuSAlg (**Fig. S2D**) are indexed at 38.1 , 44.4 , 64.5 , and 77.6 representing (111), (200), (220), and (311) crystallographic planes of face centered cubic AuNPs. **Fig. S2E** shows the XRD patterns of CNNs and BNNs. There are two diffraction peaks in CNNs around 13.2° and 26.7° , which are indexed to (100) and (002) planes representing the tri-s-triazine unit. BNNs showed a dominant peak at 26.5° , which corresponds to the (002) plane and an interlayer distance of 3.341 \AA .⁴ XRD patterns of AgFFG and AuFFG (**Fig. S2F**) showed four distinct diffraction planes (111), (200), (220), (311), and five distinct planes (111), (200), (220), (311), (222) of cubic face-centered silver and gold, respectively. XRD data indicates the successful formation of metal/FFG nanocomposite material.

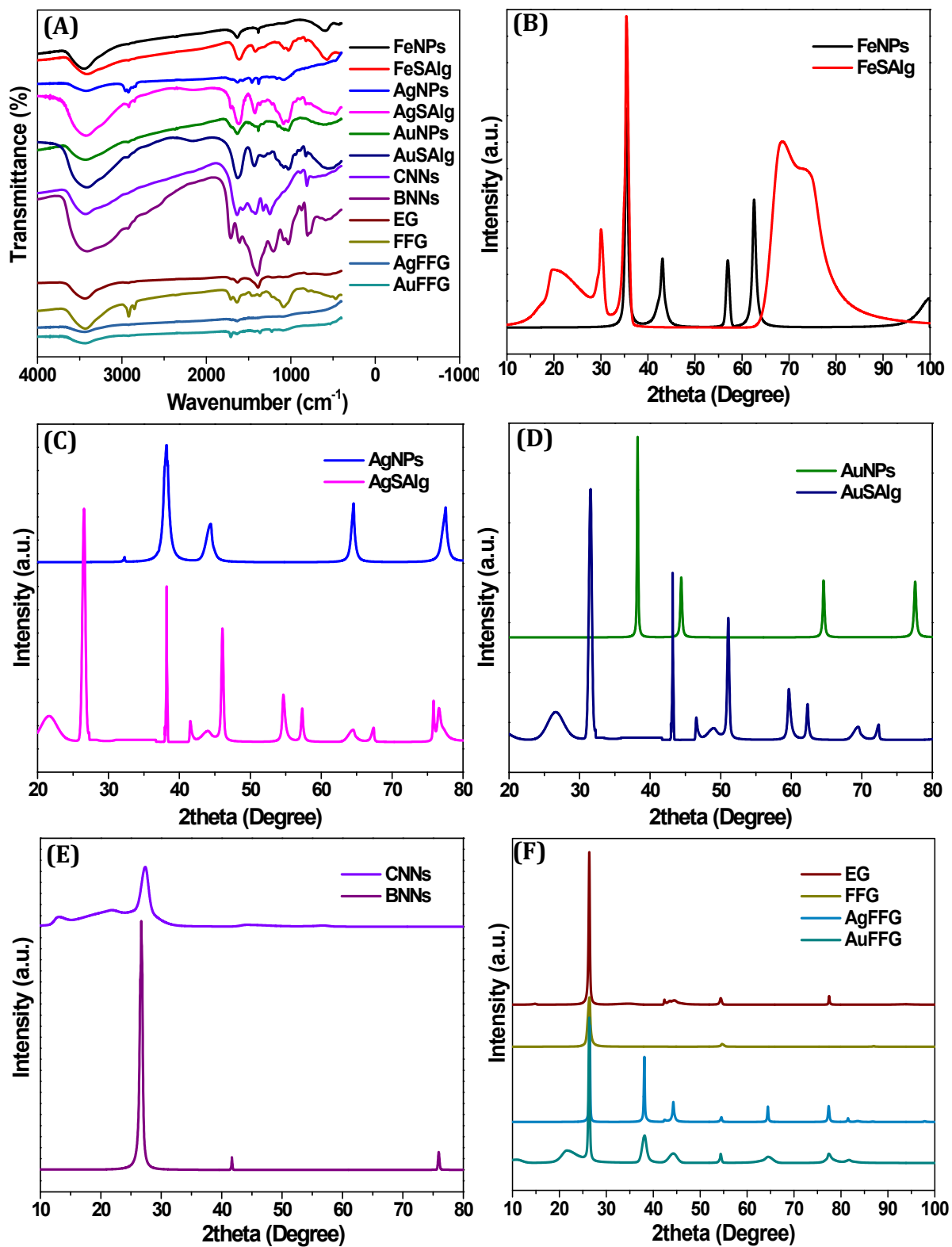


Fig. S2. (A) FTIR of nanomaterials and XRD patterns of (B) FeNPs and FeSAIg; (C) AgNPs and AgSAIg; (D) AuNPs and AuSAIg; (E) CNNs and BNNs; (F) EG, FFG, AgFFG, and AuFFG.

(C) XRD analysis of raw and all treated CC samples

XRD analysis was conducted to determine the degree of crystallinity for raw and all treated CC samples using high power X-ray diffractometer. Table S4 demonstrates the XRD analysis of raw, alkali-treated, enzyme-treated, and enzyme+FFG-treated CC biomass samples. From the obtained XRD patterns, the crystallinity index (CrI %) of all samples was calculated according to Segal et al.'s method (as described in the experimental section). The CrI % of raw and all treated CC samples was 47.93% for raw biomass, 80.29% for alkali-treated biomass, 90.82% for enzyme-treated CC, and 73.71% for enzyme-FFG treated CC (Table S4). Alkali pretreatment removed lignin and hemicellulose, increasing the crystallinity (80.29%) compared to raw CC (47.93%). We compared the effect of the cellulose crystallinity of raw and alkali-treated CC samples on the activity of the *Fusarium verticillioides* enzymes used in hydrolysis of biomass samples. We hydrolyzed these substrates using fungal enzymes at 50 °C. Hydrolysis data (Fig. 2) exhibited higher sugar release in case of alkali-treated CC sample (with 80.29 % crI) compared to raw CC sample (with 47.93% crI). The correlation between the hydrolysis and crystallinity of both raw and alkali-treated CC samples indicates that an increase in the crystallinity index improves the accessibility of the biomass samples. Alkali-treated CC sample showed higher accessibility towards enzymes than raw sample with lower crI. This observation corroborated well with previously reported studies.^{10,11}

Further, the enzyme-treated CC exhibited slight increase in crystallinity due to the enzymatic partial degradation of residual hemicellulose in the alkali-treated CC cellulose. There are several reports indicating the increase in crystallinity after enzymatic pretreatment of LCB materials.^{10,12} The achieved results were corroborated with the reported studies on cellulose isolation from CC where % crystallinity increased after treating the biomass with microwave irradiation.¹³

As discussed above, cellulose isolated after alkali treatment exhibited an increase in crystallinity compared to the raw CC and other treated samples. Further, we calculated the crystallite size of all samples, which showed the increase in size compared to the raw CC as depicted in Table S4. Alkali treatment increased the crystallite size of raw CC substrates to 54.8 nm which is remarkable. The increasing trend of cellulose crystallite size was in good agreement with the increase in cellulose crystallinity for all treated biomass samples except enzyme-treated CC (34.4 nm). Interestingly, the enzyme+FFG-treated CC exhibited the increase in crystallite size (77.5 nm) due to the action of FFG on biomass components (Table

S4). These obtained results are in accordance with the reported studies on the increase in crystallite size after different treatments of oil palm's fruit bunches.¹⁴

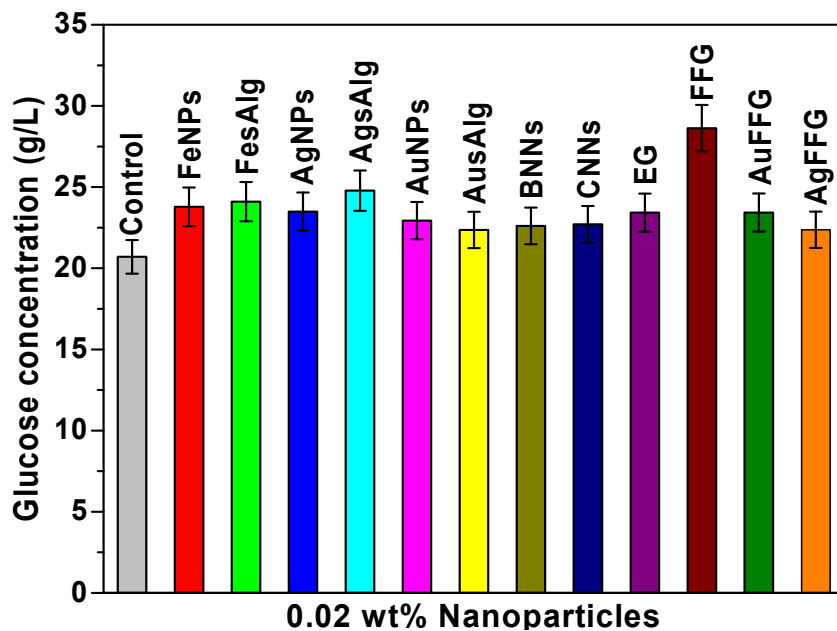


Fig. S3. Screening of nanoparticles for increased hydrolysis of corn cob derived cellulose.

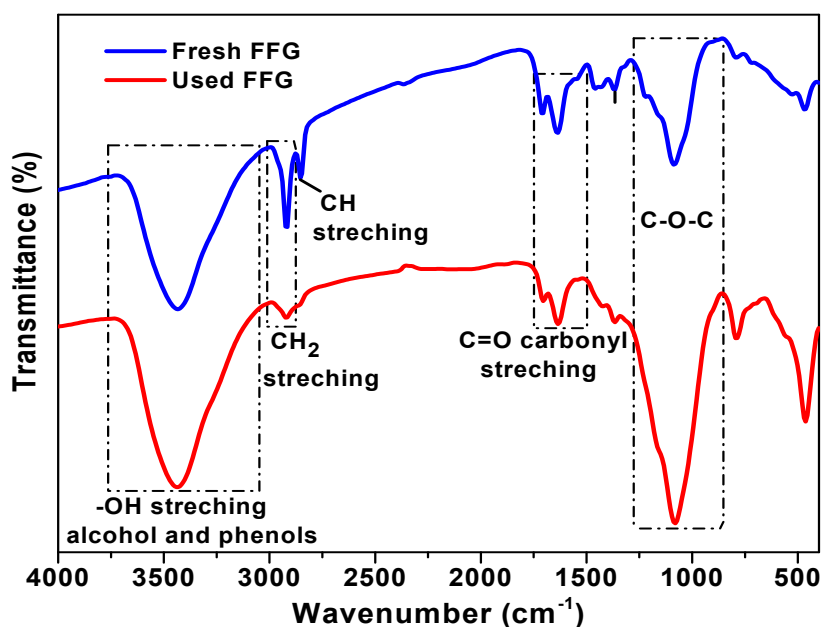


Fig. S4. Comparative FTIR analysis of used FFG (obtained after bioethanol fermentation) with new (unused) FFG to confirm the reduction of functional groups.

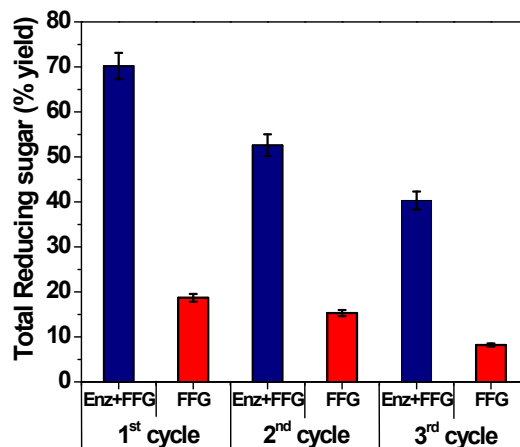


Fig. S5. Total reducing sugar profile obtained after corn cob-derived cellulose hydrolysis using enzyme + used FFG (blue) and only used FFG (red).

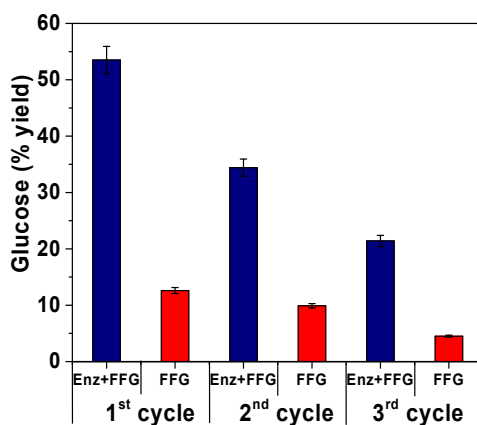


Fig. S6. Recycling of used FFG: Glucose (% yield) profile obtained after corn cob-derived cellulose hydrolysis using enzyme+used FFG (blue) and only used FFG (red).

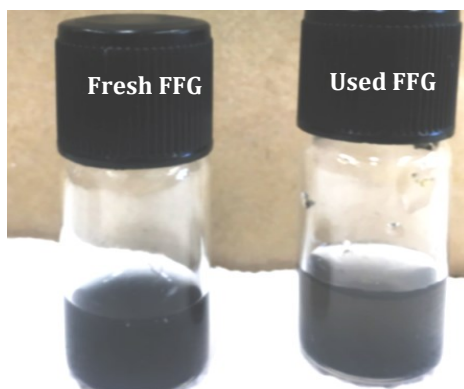


Fig. S7. Comparison of dispersion of fresh FFG and used FFG in water showing partition between water and used FFG, indicating immiscibility (due to the partial reduction of surface functional groups on FFG) which is not observed in fresh FFG.

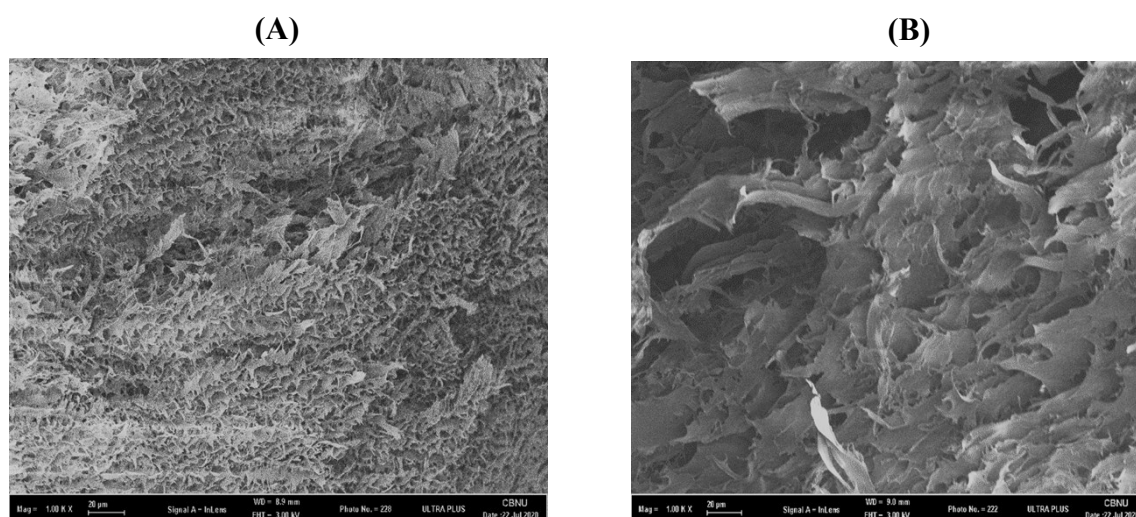


Fig. S8. SEM images of FFG/PVA aerogel (A) which shows a highly porous structure compared to neat PVA aerogel (B).

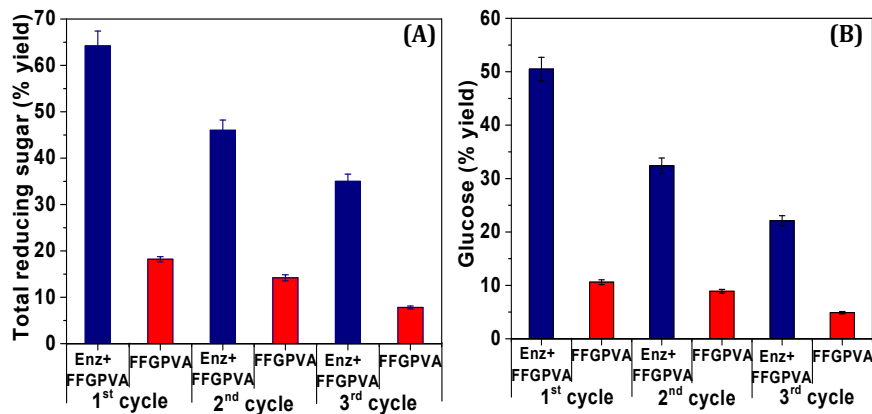


Fig. S9. Recycling of used FFG/PVA: Total reducing sugar (A) and glucose (B) profile obtained after corn cob-derived cellulose hydrolysis using enzyme+used FFG/PVA (blue) and only used FFG/PVA (red).

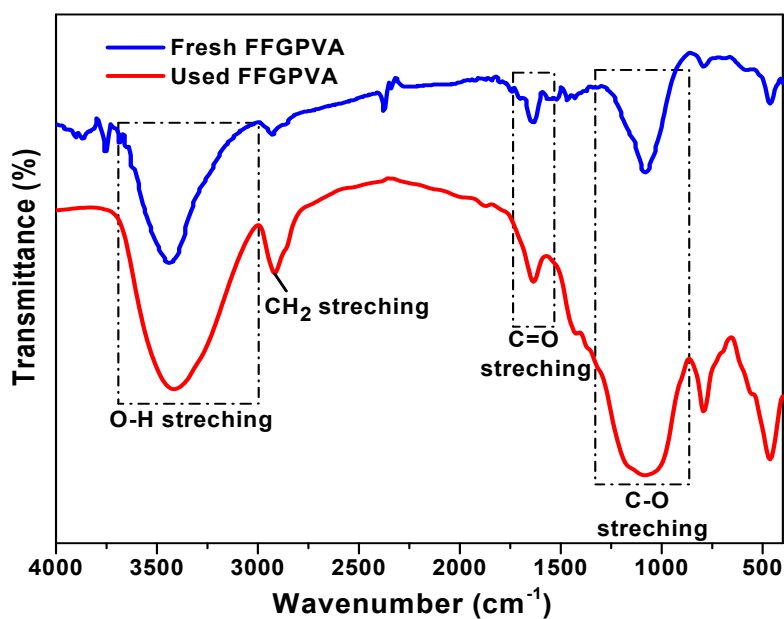


Fig. S10. FTIR analysis of fresh FFG/PVA and used FFG/PVA during hydrolysis of corn cob-derived cellulose

Table S1

Biochemical composition of raw and alkali-treated corn cob biomass

Pretreatment process	Biochemical composition (% w/w)		
	Cellulose	Hemicellulose	Lignin
Untreated corn cob	38.5 ± 1.55	34.2 ± 1.34	12.1 ± 0.81
Alkali-treated corn cob	68.7 ± 2.52	11.4 ± 0.78	3.56 ± 0.31

Values of the chemical composition represent the mean standard deviation of three replicates.

Table S2

EDS data of all nanomaterials used for the current study

Nanomaterial	Weight percentage of components (%)				
FeNPs	Fe	C	O	Cl	
	69.97	4.56	24.90	0.56	
FeSAlg	Fe	C	O	Ca	Cl
	38.74	20.80	19.45	10.37	10.64
AgNPs	Ag	C	O		
	85.17	4.07	10.75		
AgSAlg	Ag	C	O	Na	
	42.26	17.06	39.57	1.11	
AuNPs	Au	C	O		
	87.34	11.05	1.61		
AuSAlg	Au	C	O	Ca	Cl
	2.47	24.42	34.95	18.36	19.80
BNNs	B	N	C	O	
	36.95	40.65	14.17	7.52	
CNNs	C	N			
	34.12	65.88			
EG	C	O			
	96.72	3.28			
FFG	C	O			
	83.36	16.64			
AgFFG	Ag	C	O		
	9.44	83.66	6.90		
AuFFG	Au	C	O		
	1.30	91.76	6.94		

Table S3

The energy of the hydrogen bonds and hydrogen bonding distance for studied samples

Biomass Samples	Hydrogen bonding energy (EH) (kJ/mol)	Hydrogen bonding distance (R) (Å)
Raw corn cob	2.01	2.81
Alkali-treated corn cob	2.09	2.81
Enzyme-treated corn cob	2.15	2.81
FFG-treated corn cob	2.22	2.80

Table S4

Percent (%) crystallinity and crystallite sizes (nm) of raw and treated corn cob biomass samples

Biomass samples	Crystallinity index (CrI) (%)	Relative increase/decrease in crystallinity (%)	Crystallite size (nm)
Raw corn cob	47.93	-	-
Alkali-treated corn cob	80.29	67.51	54.87 ± 2.31
Enzyme-treated corn cob	73.71	-	34.47 ± 1.41
FFG-treated corn cob	90.82	13.24	77.52 ± 3.39

References:

1. A. R. Deshmukh, A. Gupta and B. S. Kim, *Biomed Res. Int.*, 2019, **2019**, 1714358.
2. A. R. Deshmukh, H. Aloui and B.S. Kim, *J. Clean. Prod.*, 2020, **270**, 122339.
3. N. Cheng, J. Tian, Q. Liu, C. Ge, A. H. Qusti, A. M. Asiri, A. O. Al-Youbi and X. Sun, *ACS Appl. Mater. Interfaces*, 2013, **5**, 6815–6819.
4. A. R. Deshmukh, J.W. Jeong, S. J. Lee, G.U. Park and B.S. Kim, *ACS Sustain. Chem. Eng.*, 2019, **7**, 17114–17125.
5. B. K. Salunke and B. S. Kim, *RSC Adv.*, 2016, **6**, 17158–17162.
6. A. R. Deshmukh, H. Aloui, C. Khomlaem, A. Negi, J. H. Yun, H. S. Kim and B.S.

- Kim, *Food Chem.*, 2021, **337**, 127777.
7. W. Tan, F. Dong, J. Zhang, X. Zhao, Q. Li and Z. Guo, *J. Agric. Food Chem.*, 2019, **67**, 2530–2539.
 8. S. Aryal, M. K. Baniya, K. Danekhu, P. Kunwar, R. Gurung and N. Koirala, *Plants*, 2019, **8**, 96.
 9. J. Wen, B. K. Salunke and B. S. Kim, *J. Chem. Technol. Biotechnol.*, 2017, **92**, 1428–1435.
 10. M. Yoshida, Y. Liu, S. Uchida, K. Kawarada, Y. Ukagami, H. Ichinose, S. Kaneko and K. Fukuda, *Biosci. Biotechnol. Biochem.*, 2008, **72**, 805–810.
 11. S. Park, J. O. Baker, M. E. Himmel, P. A. Parilla and D. K. Johnson, *Biotechnol. Biofuels*, 2010, **3**, 10.
 12. R. Banerjee, A. D. Chintagunta and S. Ray, *J. Clean. Prod.*, 2017, **149**, 387–395.
 13. M. Li, Y. L. Cheng, N. Fu, D. Li, B. Adhikari and X. D. Chen, *Int. J. Food Eng.*, 2014, **10**, 427–436.
 14. A. Kristiani, N. Effendi, Y. Aristiawan, F. Aulia and Y. Sudiyani, *Energy Procedia*, 2015, **68**, 195–204.